Authors' response to review of "Northern high-latitude permafrost and terrestrial carbon response to solar geoengineering" by Chen et al.

We thank your constructive comments, which help us clarify and greatly improve the manuscript. In the following, comments from the referees are in black, our responses are in blue.

Referee #1

The authors used a suit of models to explore the potential impact of solar engineering on permafrost carbon dynamics. They mainly found that the permafrost carbon feedback will be greatly inhibited in the scenario of solar engineering, and the permafrost ecosystems remains a carbon sink and the solar engineering will delay the transition of ecosystem carbon cycle from sink to source.

First, the historical simulations have a large deviation from the observed permafrost in terms of area and active layer thickness. The model evaluation needs to be performed in a great detail. Such model deficiency could definitely introduce significant biases into our understanding of the solar engineering impact on the permafrost dynamics. Whether these biases would undermine the main results and conclusions are yet to be determined. The authors should explore the model biases and their potential sources, and discuss the potential impact of these biases on the results. Such model biases would also be present in the simulated terrestrial carbon components such as NPP and ecosystem respiration.

Thanks for your comments. We have taken great care to analyze the model results, and have added a completely new group of land-only simulations with a state-of-the-art land surface model to examine the responses of northern high-latitude permafrost and terrestrial carbon, the results of land-only simulations are compared with that of the full-coupled earth system models (ESMs) simulations. Both groups of experiments support the following conclusions: (1) two solar geoengineering scenarios (G6solar and G6sulfur) can delay the northern high-latitude permafrost degradation under ssp585 but can not restore it from the ssp585 to ssp245 levels, (2) G6solar and G6sulfur tend to produce deeper active layer than ssp245 and expose more thawed soil organic carbon (SOC) due to robust residual high-latitude warming, (3) the turnover times of SOC decline slower under G6solar and G6sulfur than ssp585 and faster than ssp245, (4) G6solar and G6sulfur preserve more SOC than ssp585 over the northern high-latitude permafrost region. Although two groups of simulations agree that G6solar and G6sulfur would preserve more SOC than ssp585 over the northern high-latitude permafrost region, the ESMs simulations project a SOC gain, whereas the land-only simulations project a SOC loss. The opposite SOC change projected by the two groups of simulations is ascribed to their differences in baseline soil carbon stocks over the permafrost region.

We would like to answer your comments in more detail below, our reply includes two parts:

(1) Biases in the ESMs simulated permafrost extent and SOC in the permafrost region and their causes

In the full-coupled ESMs simulations, the soil temperatures derived permafrost extent ranges from 2.4 million km^2 (IPSL-CM6A-LR) to 19.0 million km^2 (CNRM-ESM2-1) during the period 1960-1990, it is considerably different from the range (12.1-17.5 million km^2) derived from the MAAT, and it is also different from the observational estimate (12.21 to 16.98 million km^2, Zhang et al., 2000) for the same period. The baseline soil carbon stock in the permafrost region ranges from 48.5 Pg C (IPSL-CM6A-LR) to 847.3 Pg C (CESM2-WACCM), and the soil carbon stocks in four of five models are considerably smaller than the observational estimate for top 3 m soil of 1091.3 Pg C according to the NCSCDv2 dataset. Several existing studies have evaluated the permafrost physics and soil carbon simulations of CMIP6 models in detail, such as Burke et al. (2020) and Varney et al. (2022). Both studies include the five ESMs (or their land components) used in this study.

To aid the analysis in this study, we compared the near-surface air temperatures, soil temperatures at 2 m depth, winter and summer thermal offsets in the baseline period 1995-2014 to explain the insulating impacts of snow and surface litter on soil freezing and thawing (Figure R1).

The thermal offsets are diagnosed as the difference between soil temperature at 0.2 m depth and near-surface air temperature. The snow insulation simulated by the models depends on the number of snow layers and snow processes represented in its snow scheme as well. The deviation of simulated permafrost states from the observation can be ascribed mainly to the biases in the simulated near-surface air temperature, thermal offsets of snow and surface litter layers, and hydrothermal processes. All five ESMs adopt multi-layered snow schemes and consider the thermal effects of soil organic matter, but no explicit litter layer (Table 1 in the revised manuscript), the thermal insulation mainly comes from snowpack and soil organic matter.

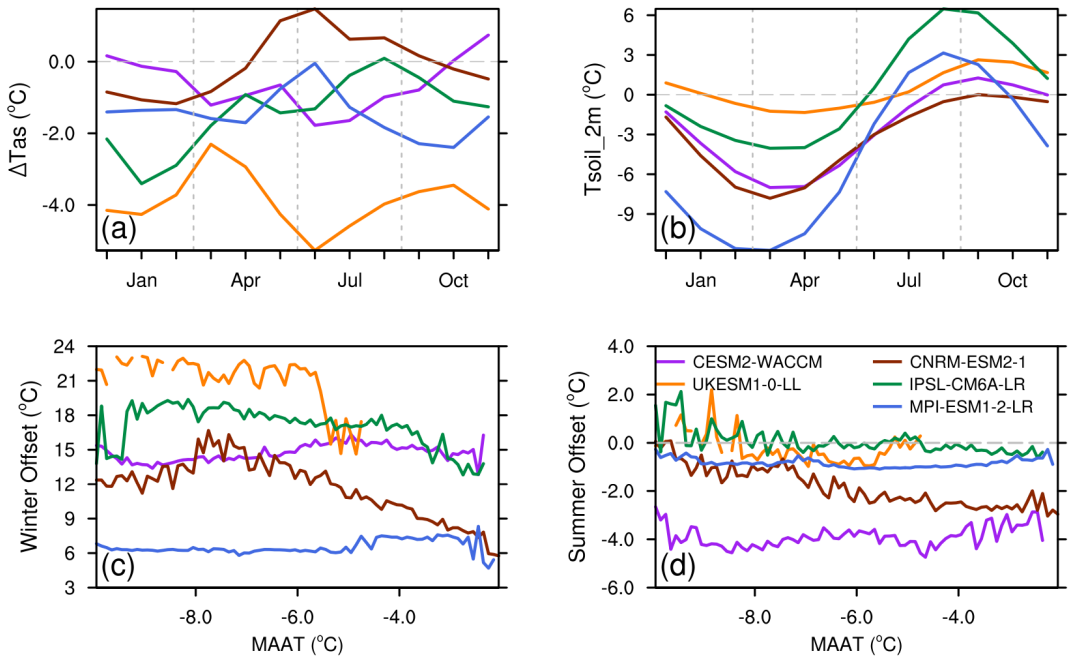

Figure R1. Climatological monthly near-surface air temperature biases, monthly soil temperatures at 2 m depth and thermal offsets of each ESM. Panel (a) shows the biases in the simulated temperature compared with the observation dataset from Climatic Research Unit gridded Time Series Version 4 (CRU Ts v4, Harris et al., 2020). Panel (b) shows the simulated climatological monthly soil temperatures at 2m depth. Panel (c) and (d) show the median values of thermal offsets vs mean annual air temperature (MAAT) in winter and summer. The thermal offset is calculated as the differences between soil temperature at 0.2 m depth and near-surface air temperature. Only grid cells where the winter mean near-surface air temperatures are between -25 and -15 °C during the baseline period 1995-2014 are shown.

For UKESM1-0-LL, it tends to underestimate near-surface air temperature year-round (Figure R1a), but its recently added multilayered snow scheme produces a too large snow thermal insulation in winter (Figure R1b). In addition, UKSEM1-0-LL adopts a shallow soil depth of only 3 m with the node depth of bottom layer at 2 m. As a result, UKESM1-0-LL can not properly simulate soil temperatures in northern high-latitude and have ALT around 2 m irrespective of MAAT (Burke et al., 2020). IPSL-CM6A-LR and MPI-ESM1-2-LR show relatively smaller deviation in near-surface air temperature (Figure R1a), but two models simulate very different permafrost extents (2.4 and 13.6 million km^2 for the period 1960-1990) according to the soil temperatures. Both of them do not consider the latent heat of water-phase change (Burke et al., 2020) and have weak thermal insulation of top surface layer in summer (Figure R1d), these tend to have the ground thawed quickly in the summer. However, due to the compensation effects of snow thermal insulation, MPI-ESM1-2-LR simulates colder soil temperatures than IPSL-CM6A-LR (Figure R1b) and produces a much large permafrost extent because MPI-ESM1-2-LR has much weaker snow thermal insulation than IPSL-CM6A-LR (Figure R1c).

For the underestimated SOC in the northern permafrost region, the main cause is that most of CMIP6 ESMs lack of adequate representation of permafrost carbon cycle (Melnikova et al., 2020; Varney et al., 2022), such as vertically resolving SOC and cryoturbation mixing on vertical SOC transportation, which are important processes to accumulate permafrost carbon stock and further

affects the magnitude of cumulative carbon decomposition (Koven et al., 2009; 2010). As Burke et al. (2020) and Varney et al. (2022) have analyzed the related issues in details, we added a short explanation and brief discussion in the revised manuscript (L207-217 and L597-609).

(2) Comparing the ESMs simulations with the anomaly forcing land model simulations

To understand the impacts of the above ESMs biases on studying the response of northern high-latitude permafrost region, we use the anomaly forcing method to drive the latest Community Land Model version 5 (CLM5) with near-surface climate change signals derived from each ESM's future scenario simulations. The anomaly forcing method can effectively capture the relative changes between scenarios in terms of near-surface climate fields required to drive an offline land model. This method has been used by the Permafrost Carbon Network model intercomparison project (McGuire et al., 2018). Comparing the results of the anomaly forcing CLM5 simulations and the ESMs simulations is helpful to understand the main sources of the uncertainties in the simulated responses of northern high-latitude permafrost and terrestrial carbon under solar geoengineering scenarios.

The CLM5 is a state-of-the-art land surface model that includes substantial processes associated with permafrost simulation, such as canopy snow processes, cryoturbation, decomposition limitation for frozen soils, vertically resolved soil carbon content (Lawrence et al., 2018). CLM5 can reasonably reproduce historical permafrost extent and soil carbon storage in northern high-latitude permafrost region (Lawrence et al., 2019). CLM5 offers a built-in function supporting the anomaly forcing method by applying precalculated future monthly anomaly signals to user-defined historical sub-daily reference forcing data (Lawrence et al., 2015). In the newly added experiments, monthly anomaly forcing datasets are created for each ESM's four future climate scenarios (G6solar, G6sulfur, ssp245 and ssp585) against their corresponding historical simulation during the period 2005-2014, including temperature, radiation, precipitation, pressure, wind, and specific humidity. CLM5 reconstructs new sub-daily forcing data by applying these precalculated monthly anomaly forcing on top of the 3-houly Global Soil Wetness Project forcing dataset (GSWP3, http://hydro.iis.u-tokyo.ac.jp/GSWP3/), which is also used to drive CLM5 for its spin-up and historical simulation from 1850 to 2014 in this study. The pertinent contents under Section 2 (Data and methods) have been updated in the revised manuscript (L127-145).

In the CLM5 historical simulation driven by GSWP3 forcing dataset, the simulated permafrost area is 12.3 million km^2 for the period 1960-1990, which is comparable to 12.21-16.98 million km^2 from observation (Zhang et al., 2000), and multi-model mean of 13.9 million km^2 derived from the MAAT in this study. The simulated soil carbon storage in the northern high-latitude permafrost region is 1089.8 Pg C, a reasonable amount compared to the observational estimate of 1035 Pg C for the top 3 m soil (Hugelius et al., 2014). Furthermore, the CLM5 simulations can reproduce the residual warming at 2 m depth soil under G6solar and G6sulfur relative to ssp245 according to the ESMs simulations. In the baseline $PF_{50\%}$ region over Northern Eurasia, the soil at 2 m depth shows 0.2±0.3 and 0.8±0.8 ºC residual warming in winter, 0.3±0.2 and 0.6±0.7 ºC residual warming in summer, respectively under G6solar and G6sulfur relative to ssp245. The CLM5 simulations show similar residual warming at 2 m depth soil, with 0.2±0.3 and 0.7±0.7 ºC in winter, 0.2±0.2 and 0.6±0.5 ºC in summer under G6solar and G6sulfur respectively with respect to ssp245.

The spatial pattern of changes in ALT under G6solar and G6sulfur relative to ssp245 are similar for the CLM5 simulations and the ESMs simulations based on CESM2-WACCM, CNRM-ESM2-1 and MPI-ESM1-2-LR. The other two ESMs were excluded in the ALT related analysis due to their too small permafrost extent (IPSL-CM6A-LR) or too shallow soil depth (UKESM1-0-LL). The estimation of SOC thaw based on CESM2-WACCM simulations is also similar to that from the CLM5 simulations and the pertinent conclusions remain unchanged. These results suggest that we can use the CLM5 simulated changes in ALT and SOC to better study how the northern high-latitude permafrost region would response under solar geoengineering scenarios. In light of this, we replaced the ALT related analysis based on CESM2-WACCM, CNRM-ESM2-1 and MPI-ESM1-2-LR with that from the CLM5 simulations. Please see the revised Figure 3, Figure 8 and main text at L260-272 and L558-564.

We also compared the permafrost extent derived from the ESMs simulated MAAT and that derived from the CLM5 simulated soil temperatures. Our results show that the permafrost extent derived from the soil temperatures retreats a litter slower than the area of $PF_{50\%}$ derived from the MAAT under G6solar, G6sulfur and the other two climate scenarios. Their differences in the permafrost retreating speed and remnant permafrost area are mainly due to their methodological differences in detecting existence of permafrost. The pertinent paragraph was added at L284-302.

For the carbon fluxes and carbon storages, we added a new table (Table 2 in the revised manuscript) and revised Figure 4 to show changes in NPP, Rh, NEP, vegetation, soil and terrestrial carbon storages during the period 2080-2099 relative to the baseline period 1995-2014 in both the CLM5 simulations and the ESMs simulations. During the baseline period in the permafrost region, both CLM5 and ESMs simulate a slightly larger NPP (2.4 Pg C yr^{-1} for CLM5, 2.7±0.7 Pg C yr^{-1} for ESMs) than Rh (2.2 Pg C yr^{-1} for CLM5, 2.5±0.6 Pg C yr^{-1} for ESMs). The more rapid growth in Rh than NPP in the CLM5 simulations leads to decreases in NEP. In contrast, the ESMs simulated growth in Rh is slower than NPP, and NEP increases. By the end of this century, the soil carbon storage in the northern high-latitude permafrost region decreases in the CLM5 simulations, while it increases in the ESM simulations.

To explain the opposite changes in SOC between the ESMs simulations and the CLM5 simulations, the spatial changes of SOC from the CLM5 simulations and the ESMs simulations are compared (Figure 6 in the revised manuscript). The CLM5 simulations project SOC loss mainly occurs over the northernmost part of permafrost region (Figure 6, right column), where soil respiration increases considerably and NEP becomes negative (Figure 6, middle column). Whereas the ESMs simulations project SOC gain in the northernmost part of permafrost region, as the soil carbon decomposition cannot offset increased soil carbon inputs due to enhanced vegetation carbon uptake. This suggest that the projected SOC change in the northern high-latitude permafrost region depends on the baseline SOC stock, as CLM5 simulates a realistic soil carbon storage in northern high-latitude permafrost region and it is much more than the ESMs simulations. Although the CLM5 simulations and the ESMs simulations project opposite changes in SOC, however, both groups of simulations agree that soil carbon storages are higher under G6solar and G6sulfur than ssp585. The pertinent contents of the CLM5 simulations have been rephrased or supplemented in Section 3.3 and 3.4.

Table 2. Changes in NPP, Rh NEP, vegetation carbon, soil carbon, terrestrial carbon storages over the baseline permafrost region during the period 2080-2099 relative to the baseline period 1995-2014 for the anomaly forcing CLM5 simulations and the ESM simulations.

		G6solar	**G6sulfur**	**ssp245**	**ssp585**
NPP (Pg C yr^{-1})	CLM5	1.9±0.3	1.7±0.4	1.5±0.2	2.5±0.3
	ESMs	2.0±1.0	1.9±1.0	1.5±0.4	2.5±0.8
Rh (Pg C yr^{-1})	CLM5	2.2±0.5	2.3±0.6	1.8±0.4	3.6±0.5
	ESMs	1.6±0.6	1.6±0.7	1.4±0.4	2.3±0.6
NEP (Pg C yr^{-1})	CLM5	-0.5±0.2	-0.6±0.2	-0.5±0.2	-1.2±0.3
	ESMs	0.3±0.4	0.2±0.4	0.1±0.1	0.2±0.4
Vegetation C (Pg C)	CLM5	9.3±0.9	9.1±1.3	7.7±0.7	11.5±0.8
	ESMs	15.7±5.8	15.2±5.4	13.5±4.6	18.7±6.2
Soil C (Pg C)	CLM5	-14.9±7.7	-19.1±7.4	-14.6±7.1	-31.4±9.3
	ESMs	17.7±18.0	16.4±16.7	13.6±12.8	13.0±18.0
Terrestrial C (Pg C)	CLM5	-5.5±6.8	-9.9±6.5	-6.5±6.6	-20.1±8.7
	ESMs	32.2±22.3	30.6±21.2	26.1±15.2	30.8±21.5

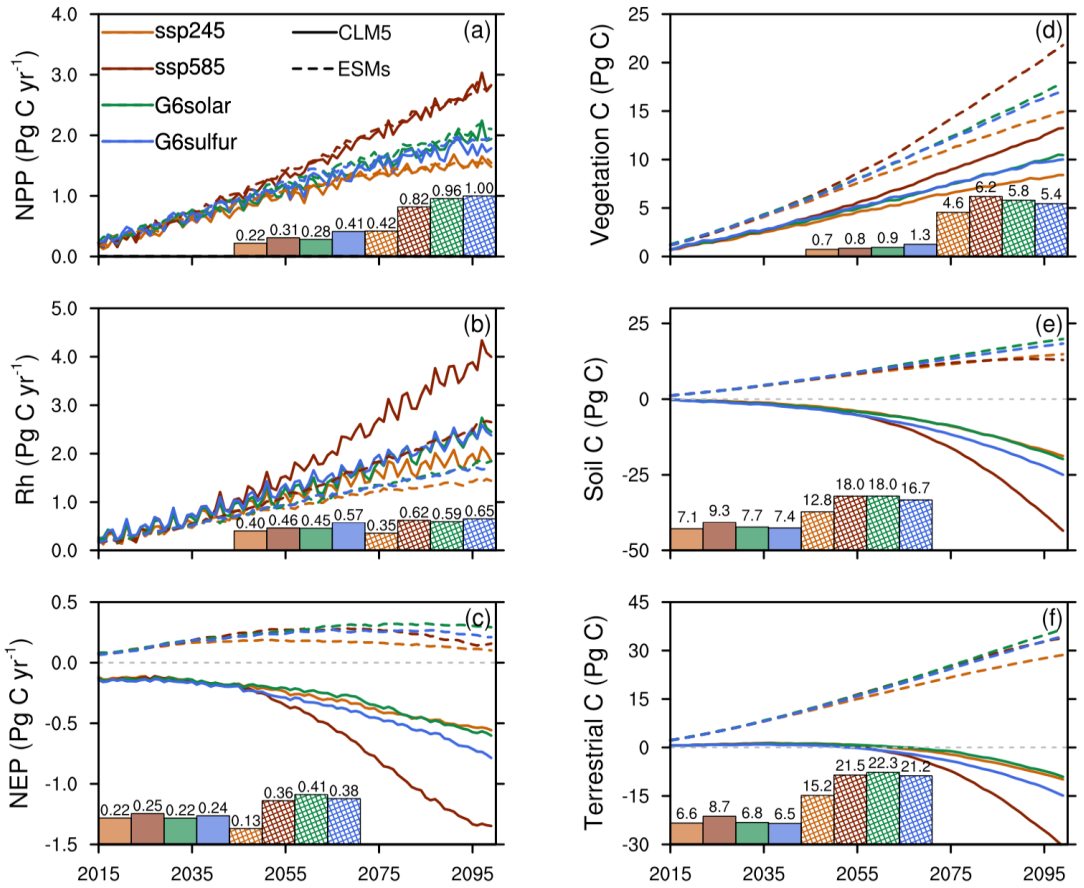

Figure 4. The multi-model mean changes of terrestrial carbon fluxes and carbon storages over the baseline permafrost region during the period 2015-2099 relative to the baseline period 1995-2014 under ssp245, ssp585, G6solar and G6sulfur. The left column shows changes in NPP (a), Rh (b) and NEP (c). The right column shows changes in vegetation (d), soil (e) and terrestrial (f) carbon storages. In each panel, bar charts denote one standard derivation from the multi-model mean averaged over the period 2080-2099, and the number above each bar denotes its magnitude. Solid lines and solid filled bars represent the anomaly forcing CLM5 simulations. Dashed lines and hatched bars represent the ESMs simulations. In panel (c), an 11-year running average is applied on NEP time series to filter its large inter-annual variation.

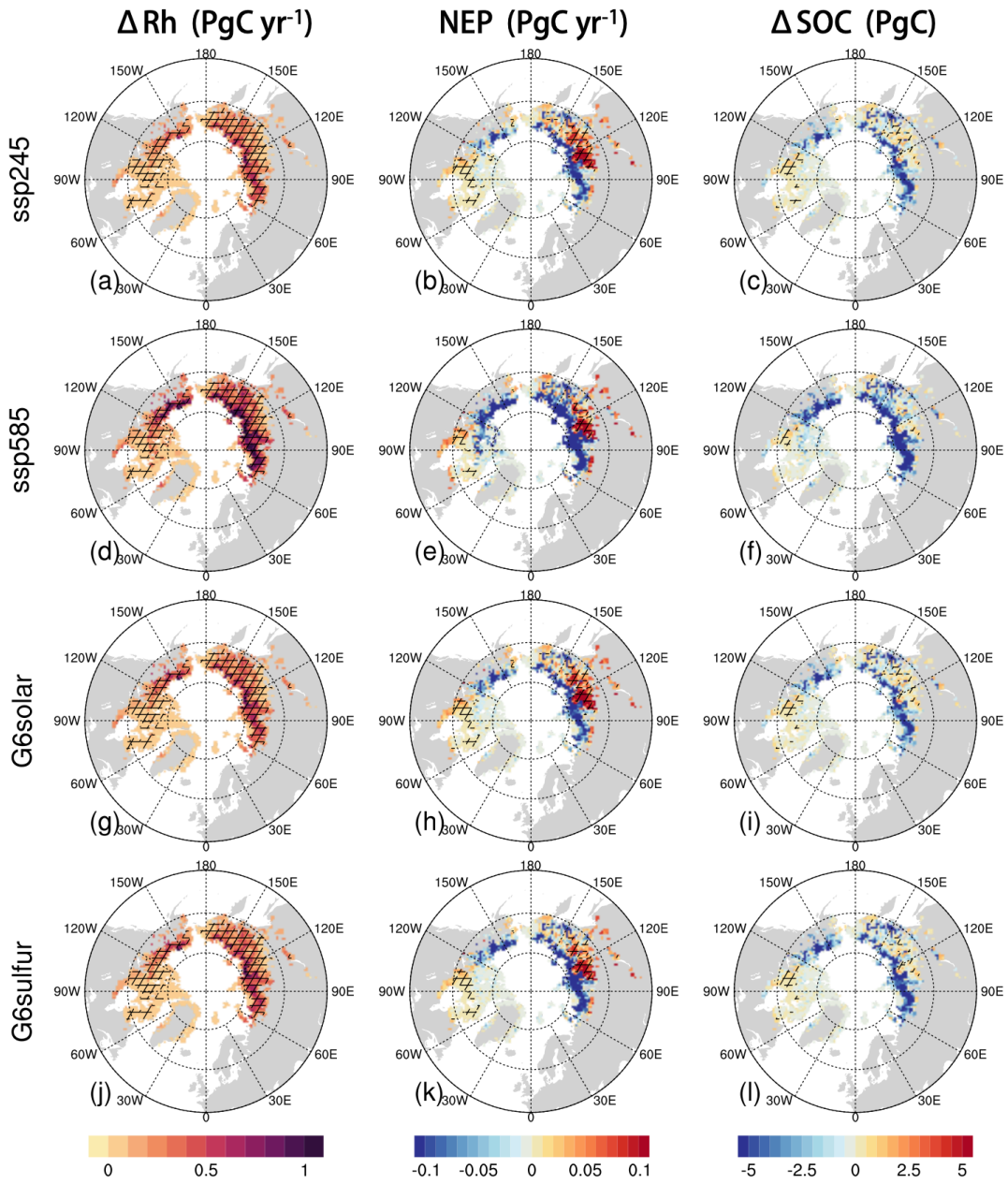

Figure 6. The multi-model mean changes in Rh (left column) and soil carbon storage (right column) averaged for the period 2080-2099 under ssp245, ssp585, G6solar and G6sulfur relative to the baseline period 1995-2014 over the baseline permafrost region in the anomaly forcing CLM5 simulations. The middle column shows NEP during the period 2080-2099. Hatched area indicates where the sign of the plotted field is same for the anomaly forcing CLM5 simulations and corresponding ESMs simulations in terms of multi-model mean.

Second, I strongly disagree with the use of permafrost carbon throughout the manuscript. Almost all of the models did not really consider the permafrost carbon processes (freezing impact on decomposition, cryoturbation etc). Moreover, the models could even fail to capture the magnitude of permafrost carbon storage. The use of observation soil carbon data in this study did not consider the yedoma carbon pool, and the results presented here would therefore definitely mislead the readers. All of the expression related to permafrost carbon should be removed, since this is nothing to do with the real permafrost carbon dynamic processes.

Thanks for your comments. In the five ESMs used in this study, only the land component (CLM5) of CESM2-WACCM considers relatively sophisticated permafrost physical and

biogeochemical processes as noted in our reply above. Other models do fail to capture the magnitude of soil carbon storage in the northern permafrost region. This is the very reason that we have carried out new experiments by using the anomaly forcing CLM5 to capture the main uncertainties in projecting the responses of northern high-latitude permafrost and terrestrial carbon under solar geoengineering.

On the centennial time scale, the soil carbon in the top 3 m depth is the most vulnerable to microbial decomposition and it controls changes in permafrost soil organic carbon stocks. The deeper yedoma contains about 327-466 Pg C of soil carbon in the present permafrost region and approximately 32 Pg C of it is stored in the upper 3 m soil (Hugelius et al., 2014; Strauss et al., 2017). The soil carbon in the yedoma deposits has not yet been throughly represented in any CMIP6 ESM (Varney et al., 2022), and more in situ research might be required to better understand its physical and biogeochemical processes and potential impacts. To avoid misleading readers, we have revised the expression of "permafrost carbon" to "near-surface permafrost soil carbon" or “soil carbon in the permafrost region”. Thank you for pointing out this aspect.

Referee #2

General comment

The authors studied how the permafrost extent and terrestrial carbon fluxes and pools are in response to two solar geoengineering scenarios, ssp245 and 585 scenarios based on CMIP6 simulations. The topic is timely and fits the scope of the journal Earth System Dynamics. The paper is well structured and the results are well illustrated in the figures. However, the authors need to put more effort to explain how the difference in surface climate between solar geoengineering scenarios and ssp245 affects soil surface temperature, NPP, and ER. Vegetation response to climate forcing plays a major role here. It is strange that G6solar and G6sulfur have lower radiation or summer temperature than ssp245, but they still have higher NPP and ER. Also, snow duration and surface litter are important insulators for soil freezing and thawing. I suggest the authors should mention these aspects in their discussion. Finally, the authors should polish the language further and avoid some grammar mistakes.

Thank you for your constructive comments. We would like to respond to your questions in the general comment as follows:

1. The authors need to put more effort to explain how the difference in surface climate between solar geoengineering scenarios and ssp245 affects soil surface temperature, NPP, and ER. Vegetation response to climate forcing plays a major role here.

Thanks for your suggestions. High-latitude near-surface air temperatures are generally higher under G6solar and G6sulfur than ssp245, especially over Northern Eurasia (Visioni et al., 2021). The impacts of differences in near-surface air temperature on soil surface temperature depends on the thermal insulation of snow and litter layers. The five earth system models (ESMs) used in this study all adopt multi-layered snow schemes and consider the thermal effects of soil organic matter, but no explicit litter layer. The largest differences between near-surface air temperature and soil surface temperature occur in winter, when the snowpack creates strong thermal insulation. In the $PF_{50\%}$ region, the differences in snow coverage and snow depth are statistically insignificant between G6solar and ssp245, while the snow depth under G6sulfur is slightly thicker than ssp245 due to more snowfall in winter (Figure 1r). However, the averaged thermal offset (measured as soil temperature at 0.2 m depth minus near-surface air temperature) over the baseline permafrost region during the period 2080-2099 are 4.0±2.4, 3.9±2.3 and 4.1±2.4 ºC for G6solar, G6sulfur and ssp245 respectively, their differences are considerably smaller than the magnitude of residual winter warming in near-surface air (0.6±0.2 ºC for G6solar, 2.1±0.8 ºC for G6sulfur). As a result, the spatial patterns of residual warming in near-surface air and 0.2 m depth soil are similar (Figure 1e vs 1i, 1f vs 1j). In winter, the magnitude of residual warming in soil at 0.2 m depth (Figure 1i-j) is relatively smaller than near-surface air (Figure 1e-f) mostly due to thermal insulation of snow layers, and the residual warming attenuates further at 2 m depth soil (Figure 1m-n). In summer, the residual warming in near-surface air (Figure 1g-h) is less pronounced in both G6solar and G6sulfur than winter. However, the residual warming in soil at 2 m depth (Figure 1p) is more pronounced than near-surface air (Figure 1h) under G6sulfur. This is due to the profound residual winter warming in near-surface air affecting the summer soil at deep layers (Burn and Zhang, 2010). The above explanations have been added in Section 3.1 (L207-229). At the same time, the Figure 1 has been revised to better illustrate the spatial pattern of residual warming in near-surface air and its impacts to soil temperature from winter to summer.

G6solar and G6sulfur have lower solar radiation and higher summer temperature, NPP and ER, compared to ssp245. By direct solar irradiance reduction and radiation reflection by stratospheric aerosol, the downward surface shortwave radiation under G6solar and G6sulfur is lower than ssp245. In contrast, both G6solar and G6sulfur have higher summer temperatures than ssp245, as decreasing insolation and increasing CO_2 modifies the vertical profiles of atmospheric temperature and atmospheric energy transport. This is the main reason for the residual near-surface warming at high latitudes under solar reduction geoengineering (Henry and Merlis, 2020). The multi-model mean near-surface air temperature under G6solar and G6sulfur is 0.4±0.1 and 0.6±0.6 ºC higher than ssp245 on annual average. Moreover, as G6solar and G6sulfur share the same CO_2

concentrations as ssp585, the stronger CO_2 fertilization effects would facilitate vegetation growth and enhance NPP increasing more than ssp245. Therefore, the higher NPP under G6solar and G6sulfur in summer relative to ssp245 is ascribed to the warmer temperatures and higher CO_2 concentration. Larger ER under G6solar and G6sulfur not only comes from more active soil carbon decomposition under warmer summer temperatures but also from larger amounts of thawed soil carbon exposed to microbial activity. The pertinent explanation has been added or rephrased in the revised manuscript (L201-202, L330-332 and L340-341).

Furthermore, the differences in NPP mirror more directly structural and parametric differences in land surface models adopted by the five ESMs, in particular the carbon assimilation scheme that depends on nutrient limitation. The models which represent land nitrogen cycle (CESM2-WACCM, MPI-ESM1-2-LR and UKESM1-0-LL) simulate similar NPP magnitudes (~ 3 Pg C yr^{-1}) during the baseline period 1995-2014. Except for CNRM-ESM2-1, NPP increases similarly under G6solar, G6sulfur and ssp245 for the other four models (Figure R2), consistent with their comparable land carbon-concentration feedback parameters (Table A1 in Arora et al., 2020). Whereas for CNRM-ESM2-1, NPP increases similarly under G6solar, G6sulfur and ssp585 (Figure R2c), probably due to its largest land carbon-concentration feedback parameter in the five ESMs (Table A1 in Arora et al., 2020). The pertinent content has been added in the revised manuscript (L451-463).

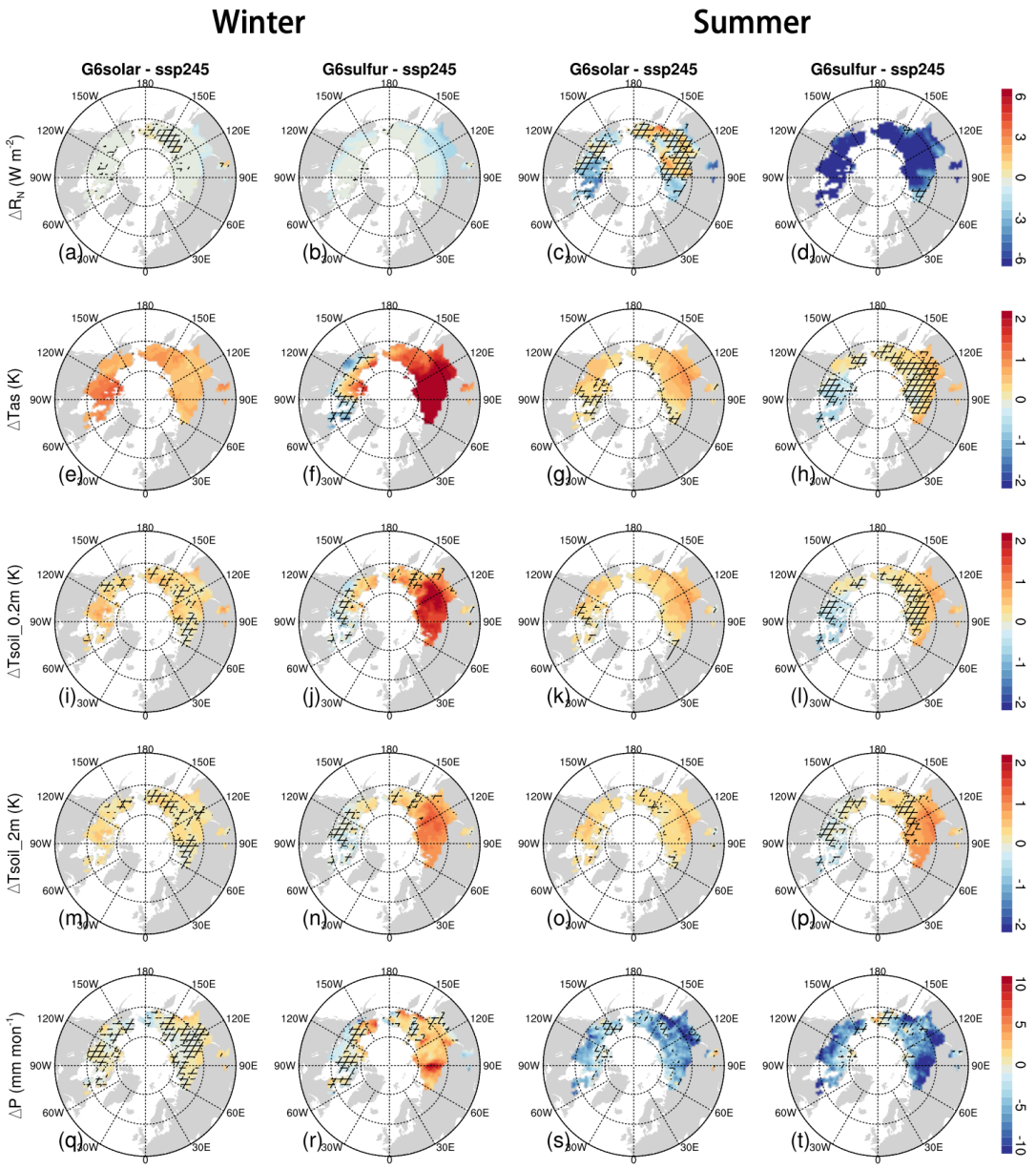

Figure 1. The multi-model mean changes of surface absorbed shortwave radiation (ΔR_N; a, b, c, d), near-surface air temperature (ΔTas; e, f, g, h), 0.2 m soil temperature (ΔTsoil_0.2m; i, j, k, l), 2 m soil temperature (ΔTsoil_2m; m, n, o, p) and precipitation (ΔP; q, r, s, t) under G6solar and G6sulfur relative to ssp245 during the period 2080-2099 over the baseline $PF_{50\%}$ region. The left two columns show changes in winter (December, January, and February), the right two columns show changes in summer (June, July, and August). The hatched area in each panel indicates where less than 80% of the ESMs (four out of five) agree on the sign of changes.

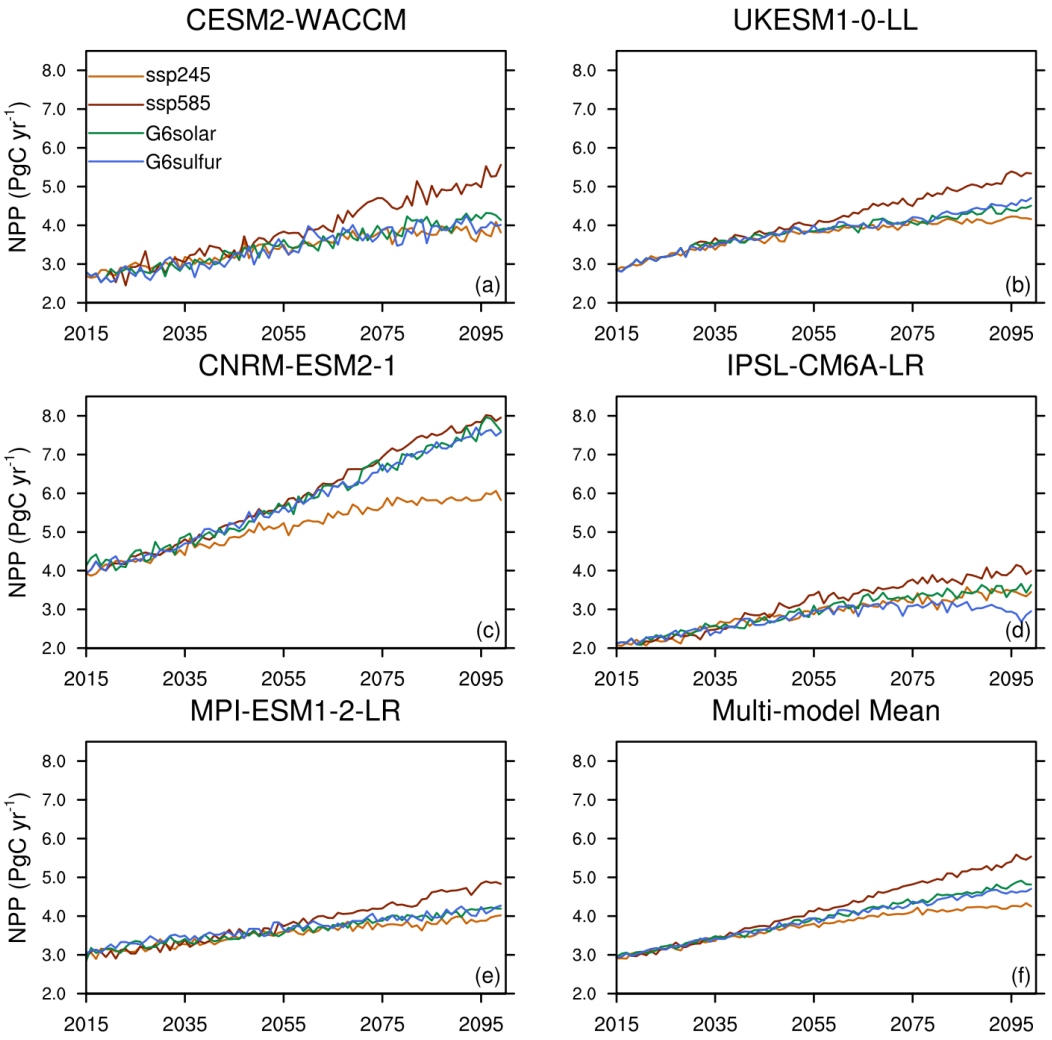

Figure R2. Changes in annual accumulated NPP (Pg C yr^{-1}) for each ESM during the period 2015-2099 under ssp245, ssp585, G6solar and G6sulfur. To illustrate the differences between models, the same range of y-axis is applied for all panels.

2. Also, snow duration and surface litter are important insulators for soil freezing and thawing.

Thanks for your comment. This is clarified and improved in the discussion. Please see our replies (Biases in the ESMs simulated permafrost extent and SOC in the permafrost region and their causes) to the first general comment raised by the other referee.

Specific comments

1. Title: to be more specific, like "two solar geoengineering scenarios".

Thanks. The title is revised to "Northern high-latitude permafrost and terrestrial carbon response to two solar geoengineering scenarios".

2. Line 18, reduce -> reduces.

Thanks. Line 18 "reduce" is revised to "reduces".

3. Line 18, "including" makes readers confused.

Agree. We rephrased Line 18 to "Solar geoengineering is a means of mitigating temperature rise and reduces some of the associated climate impacts by increasing the planetary albedo, the permafrost thaw is expected to be moderated under slower temperature rise. "

4. Line 20-23: I suggest the authors describe more clearly what four scenarios are. Are they two solar geoengineering scenarios based on the settings of ssp245 and ssp585 respectively?

Thanks. Both G6solar and G6sulfur use ssp585 as the background scenario. They reduce the net anthropogenic radiative forcing from ssp585 to ssp245 levels by solar irradiance reduction (G6solar) and stratospheric sulfate aerosol injection (G6sulfur). We revised Line 20-23 to "two solar geoengineering scenarios (G6solar and G6sulfur) based on the high emission scenario (ssp585) restore the global temperature from the ssp585 levels to the moderate mitigation scenario (ssp245) levels via solar dimming and stratospheric aerosol injection."

5. Line 25 to 30: to report results in a quantitative way.

Thanks for your suggestion. We revised Line 25-30 to "G6solar and G6sulfur preserve 4.6±4.6 and 3.4±4.8 Pg C (coupled ESMs simulations) or 16.4±4.7 and 12.3±7.9 Pg C (offline land surface model simulations) more SOC respectively than ssp585 over the northern high-latitude permafrost region. The turnover times of SOC decline slower under G6solar and G6sulfur than ssp585 and faster than ssp245. The permafrost carbon-climate feedback is expected to be weaker under solar geoengineering."

6. Line 35: "driven by Arctic amplification", this sentence has a logical mistake. More rapid warming in the north than in the south actually means Arctic amplification.

Thanks. Line 34-36 is revised to "In the past several decades, the northern high-latitude experienced greater warming than the lower latitudes, recognized as Arctic amplification, and this rapid warming trend is expected to continue in the future (Serreze and Barry, 2011; Biskaborn et al., 2019). "

7. Line 36: renders -> render.

Thanks. Line 36 "renders" is revised to "render".

8. Line 118: Is the G6sulfur run based on the setting of ssp585?

Yes. The G6sulfur run is based on the setting of ssp585. We revised it to "G6sulfur is based on ssp585 as well, whereas reduces radiative forcing from ssp585 to ssp245 levels through stratospheric aerosol injection from 10°S to 10°N along a single longitude band (Kravitz et al., 2015).". See L124-126 in the revised manuscript.

9. Line 122: You need to give some arguments on why the baseline period uses 20 years but the future period uses 10 years.

Thanks. The analysis for the future uses the last 20 years (2080-2099) of the model simulations. We have stated it in L153 under Section 2.2.

10. Line 163 and 165: How did you linearly interpolate the soil temperature from the surface? The permafrost model should be able to simulate multi-layer soil temperature.

Thank you for your question. Indeed, all the models used in this study have multi-layer soil temperatures, but the vertical discretization of the soil column is uneven amongst models, and soil temperature is only available at the discrete node depths. To derive ALT, we use piecewise linear interpolation to interpolate the monthly soil temperature data to 300 evenly spaced levels (each layer of 0.01m thickness), soil temperatures exceeding 0 °C is assumed as thawed, and the deepest thawed depth amongst the year is defined as ALT. For the evenly spaced levels located above the top soil node of model, their temperatures are assumed to be the same as the soil temperature at the top soil node. The pertinent content has been rephrased in the revised manuscript L180-182.

11. I suggest the authors add a table or time series for permafrost areal extent, which is complementary to figure 2.

Thank you for your suggestion, we have added the time series for permafrost areal extent in the revised Figure 2.

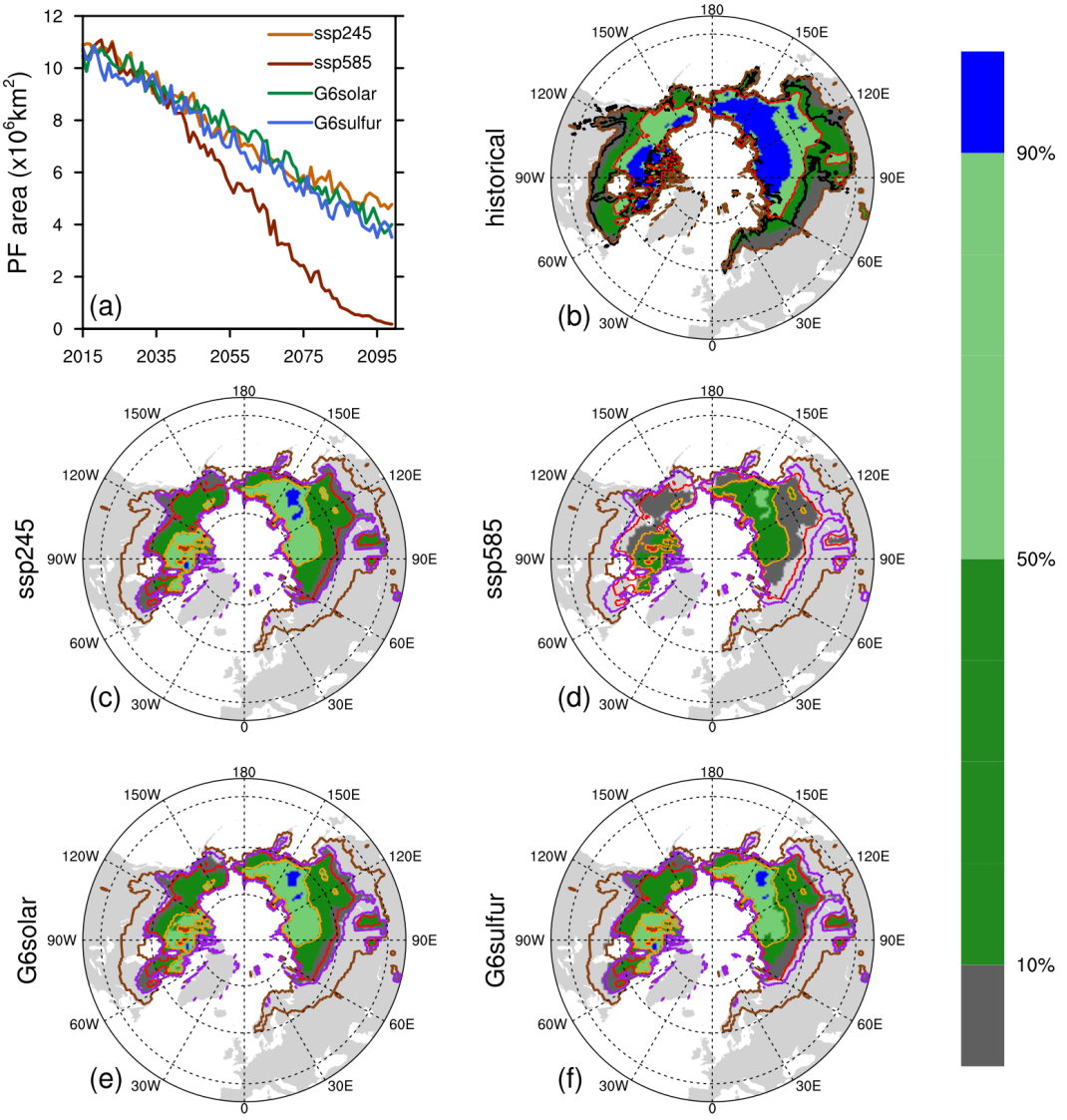

Figure 2. Permafrost area and probability derived according to the observation-based MAAT-permafrost probability relationship (Chadburn et al., 2017). Panel (a) shows change of multi-model mean area of the $PF_{50\%}$ region under ssp245, ssp585, G6solar and G6sulfur during the period 2015-2099. Panels (b-f) show multi-model mean permafrost probability (shading) and region (curves) for the last 20 years of each experiment. The black curve in (b) denotes the permafrost region defined by IPA permafrost map. The brown and purple curves denote the multi-model mean permafrost regions (permafrost probability ≥ 0.01) for historical and ssp245 simulations, respectively. The red and orange curves denote the multi-model mean permafrost regions where the permafrost probability ≥ 0.5 for historical and ssp245 simulations, respectively.

12. In Figure 3 and Figure 4, I think the authors need to explain why G6solar and G6sulfur have lower radiation and summer temperature but still higher NPP and RH, compared to ssp245.

Thanks for your comments. G6solar and G6sulfur have higher summer temperatures than ssp245, as decreasing insolation and increasing CO_2 modifies the vertical profiles of atmospheric temperature and atmospheric energy transport. The multi-model mean near-surface air temperature under G6solar and G6sulfur is 0.4±0.1 and 0.6±0.6 ºC higher than ssp245 on annual average respectively. Moreover, as G6solar and G6sulfur share the same CO_2 concentrations as ssp585, the stronger CO_2 fertilization effect would facilitate vegetation growth and enhance NPP increasing more than ssp245. Therefore, the higher NPP under G6solar and G6sulfur relative to ssp245 is ascribed to the warmer temperatures and higher CO_2 concentration. Larger RH under G6solar and G6sulfur not only comes from more active soil carbon decomposition under warmer summer temperatures but also from larger amounts of thawed soil carbon exposed to microbial activity. The pertinent content has been added in the revised manuscript (L201-202, L330-332 and L353-355).

13. Figure 6. In the caption, "G6solar, G6sulfur, and ssp585" need to be reversed in their order.

Thanks. The content of previous Figure 6 has been merged with Figure 4 in the revised manuscript to better illustrate the relationship between changes in carbon fluxes and carbon pools. Please see our reply to the next comment.

14. You should present a figure of ensemble standard deviations from each scenario in the appendix.

Thanks for your constructive suggestion. The revised Figure 4 shows the multi-model mean of terrestrial carbon fluxes and carbon stocks changes over the baseline permafrost region and their spreads (plotted as bar charts in each panel). To address the comments raised from the other referee, we conducted anomaly-forcing experiments using the latest Community Land Model version 5 (CLM5). CLM5 can reasonably reproduce historical permafrost extent and soil carbon storage in the northern high-latitude permafrost region (Lawrence et al., 2019). Figure 4 shows both the results from the ESMs simulations and the CLM5 simulations. Please see our replies (Comparing the ESMs simulations with the anomaly forcing land model simulations) to the first general comment raised by the other referee.

References:

Arora, V. K., Katavouta, A., Williams, R. G., Jones, C. D., Brovkin, V., Friedlingstein, P., Schwinger, J., Bopp, L., Boucher, O., Cadule, P., Chamberlain, M. A., Christian, J. R., Delire, C., Fisher, R. A., Hajima, T., Ilyina, T., Joetzjer, E., Kawamiya, M., Koven, C. D., Krasting, J. P., Law, R. M., Lawrence, D. M., Lenton, A., Lindsay, K., Pongratz, J., Raddatz, T., Séférian, R., Tachiiri, K., Tjiputra, J. F., Wiltshire, A., Wu, T., and Ziehn, T.: Carbon–concentration and carbon–climate feedbacks in CMIP6 models and their comparison to CMIP5 models, Biogeosciences, 17, 4173-4222, https://doi.org/10.5194/bg-17-4173-2020, 2020.

Biskaborn, B. K., Smith, S. L., Noetzli, J., Matthes, H., Vieira, G., Streletskiy, D. A., Schoeneich, P., Romanovsky, V. E., Lewkowicz, A. G., Abramov, A., Allard, M., Boike, J., Cable, W. L., Christiansen, H. H., Delaloye, R., Diekmann, B., Drozdov, D., Etzelmüller, B., Grosse, G., Guglielmin, M., Ingeman-Nielsen, T., Isaksen, K., Ishikawa, M., Johansson, M., Johannsson, H., Joo, A., Kaverin, D., Kholodov, A., Konstantinov, P., Kröger, T., Lambiel, C., Lanckman, J., Luo, D., Malkova, G., Meiklejohn, I., Moskalenko, N., Oliva, M., Phillips, M., Ramos, M., Sannel, A. B. K., Sergeev, D., Seybold, C., Skryabin, P., Vasiliev, A., Wu, Q., Yoshikawa, K., Zheleznyak, M., and Lantuit, H.: Permafrost is warming at a global scale, Nat. Commun., 10, 1-11, https://doi.org/10.1038/s41467-018-08240-4, 2019.

Burke, E. J., Zhang, Y., and Krinner, G.: Evaluating permafrost physics in the Coupled Model Intercomparison Project 6 (CMIP6) models and their sensitivity to climate change, The Cryosphere, 14, 3155-3174, https://doi.org/10.5194/tc-14-3155-2020, 2020.

Burn, C. R., and Zhang, Y.: Sensitivity of active-layer development to winter conditions north of treeline, Mackenzie delta area, western Arctic coast, in: Proceedings of the 6th Canadian Permafrost Conference, The 63rd Canadian Geotechnical Conference, Calgary, Alberta, 12-16 September 2010, http://pubs.aina.ucalgary.ca/cpc/CPC6-1458.pdf, 1458-1465, 2010.

CLM5 Documentation, https://www.cesm.ucar.edu/models/cesm2/land/CLM50_Tech_Note.pdf, last access: 30 October 2022.

Global Soil Wetness Project Phase 3 (GSWP3): http://hydro.iis.u-tokyo.ac.jp/GSWP3/, last access: 30 October 2022.

Harris, I., Osborn, T. J., Jones, P., and Lister, D.: Version 4 of the CRU TS monthly high-resolution gridded multivariate climate dataset, Scientific Data, 7, 109, https://doi.org/10.1038/s41597-020-0453-3, 2020.

Henry, M., and Merlis, T. M.: Forcing Dependence of Atmospheric Lapse Rate Changes Dominates Residual Polar Warming in Solar Radiation Management Climate Scenarios, Geophys. Res. Lett., 47, e2020GL087929, https://doi.org/10.1029/2020GL087929, 2020.

Hugelius, G., Strauss, J., Zubrzycki, S., Harden, J. W., Schuur, E. A. G., Ping, C. L., Schirrmeister, L., Grosse, G., Michaelson, G. J., Koven, C. D., O'Donnell, J. A., Elberling, B., Mishra, U., Camill, P., Yu, Z., Palmtag, J., and Kuhry, P.: Estimated stocks of circumpolar permafrost carbon with quantified uncertainty ranges and identified data gaps, Biogeosciences, 11, 6573-6593, https://doi.org/10.5194/bg-11-6573-2014, 2014.

Kravitz, B., Robock, A., Tilmes, S., Boucher, O., English, J. M., Irvine, P. J., Jones, A., Lawrence, M. G., MacCracken, M., Muri, H., Moore, J. C., Niemeier, U., Phipps, S. J., Sillmann, J., Storelvmo, T., Wang, H., and Watanabe, S.: The Geoengineering Model Intercomparison Project Phase 6 (GeoMIP6): simulation design and preliminary results, Geosci. Model Dev., 8, 3379-3392, https://doi.org/10.5194/gmd-8-3379-2015, 2015.

Lawrence, D. M., Koven, C. D., Swenson, S. C., Riley, W. J., and Slater, A. G.: Permafrost thaw and resulting soil moisture changes regulate projected high-latitude CO_2 and CH_4 emissions, Environ. Res. Lett., 10, 094011, https://doi.org/10.1088/1748-9326/10/9/094011, 2015.

Lawrence, D., Fisher, R., Koven, C. D., Oleson, K., Swenson, S., Vertenstein, M. et al., 2018, Technical

Description of version 5.0 of the Community Land Model (CLM), http://www.cesm.ucar.edu/models/cesm2/land/CLM50_Tech_Note.pdf

Lawrence, D. M., Fisher, R. A., Koven, C. D., Oleson, K. W., Swenson, S. C., Bonan, G., Collier, N., Ghimire, B., van Kampenhout, L., Kennedy, D., Kluzek, E., Lawrence, P. J., Li, F., Li, H., Lombardozzi, D., Riley, W. J., Sacks, W. J., Shi, M., Vertenstein, M., Wieder, W. R., Xu, C., Ali, A. A., Badger, A. M., Bisht, G., van den Broeke, M., Brunke, M. A., Burns, S. P., Buzan, J., Clark, M., Craig, A., Dahlin, K., Drewniak, B., Fisher, J. B., Flanner, M., Fox, A. M., Gentine, P., Hoffman, F., Keppel Aleks, G., Knox, R., Kumar, S., Lenaerts, J., Leung, L. R., Lipscomb, W. H., Lu, Y., Pandey, A., Pelletier, J. D., Perket, J., Randerson, J. T., Ricciuto, D. M., Sanderson, B. M., Slater, A., Subin, Z. M., Tang, J., Thomas, R. Q., Val Martin, M., and Zeng, X.: The Community Land Model Version 5: Description of New Features, Benchmarking, and Impact of Forcing Uncertainty, J. Adv. Model. Earth Sy., 11, 4245-4287, https://doi.org/10.1029/2018MS001583, 2019.

McGuire, A. D., Lawrence, D. M., Koven, C., Clein, J. S., Burke, E., Chen, G., Jafarov, E., MacDougall, A. H., Marchenko, S., Nicolsky, D., Peng, S., Rinke, A., Ciais, P., Gouttevin, I., Hayes, D. J., Ji, D., Krinner, G., Moore, J. C., Romanovsky, V., Schädel, C., Schaefer, K., Schuur, E. A. G., and Zhuang, Q.: Dependence of the evolution of carbon dynamics in the northern permafrost region on the trajectory of climate change, Proceedings of the National Academy of Sciences, 115, 3882-3887, https://doi.org/10.1073/pnas.1719903115, 2018.

Melnikova, I., Boucher, O., Cadule, P., Ciais, P., Gasser, T., Quilcaille, Y., Shiogama, H., Tachiiri, K., Yokohata, T., and Tanaka, K.: Carbon Cycle Response to Temperature Overshoot Beyond 2°C: An Analysis of CMIP6 Models, Earth's Future, 9, e2020EF001967, https://doi.org/10.1029/2020EF001967, 2021.

Serreze, M. C., and Barry, R. G.: Processes and impacts of Arctic amplification: A research synthesis, Global Planet. Change, 77, 85-96, https://doi.org/10.1016/j.gloplacha.2011.03.004, 2011.

Strauss, J., Schirrmeister, L., Grosse, G., Fortier, D., Hugelius, G., Knoblauch, C., Romanovsky, V., Schädel, C., Schneider Von Deimling, T., Schuur, E. A. G., Shmelev, D., Ulrich, M., and Veremeeva, A.: Deep Yedoma permafrost: A synthesis of depositional characteristics and carbon vulnerability, Earth-Sci. Rev., 172, 75-86, https://doi.org/10.1016/j.earscirev.2017.07.007, 2017.

Visioni, D., MacMartin, D. G., Kravitz, B., Boucher, O., Jones, A., Lurton, T., Martine, M., Mills, M. J., Nabat, P., Niemeier, U., S Ef Erian, R., and Tilmes, S.: Identifying the sources of uncertainty in climate model simulations of solar radiation modification with the G6sulfur and G6solar Geoengineering Model Intercomparison Project (GeoMIP) simulations, Atmos. Chem. Phys., 21, 10039-10063, https://doi.org/10.5194/acp-21-10039-2021, 2021.

Zhang, T., Heginbottom, J. A., Barry, R. G., and Brown, J.: Further statistics on the distribution of permafrost and ground ice in the Northern Hemisphere, Polar geography (1995), 24, 126-131, https://doi.org/10.1080/10889370009377692, 2000.